



Contents lists available at ScienceDirect

Biotechnology Advances

journal homepage: [www.elsevier.com/locate/biotechadv](http://www.elsevier.com/locate/biotechadv)

## *In vitro* and *in vivo* bioactivity of CoBlast hydroxyapatite coating and the effect of impaction on its osteoconductivity

Fei Tan<sup>a,b,c</sup>, Mariam Naciri<sup>a,b</sup>, Denis Dowling<sup>d</sup>, Mohamed Al-Rubeai<sup>a,b,\*</sup>

<sup>a</sup> School of Chemical and Bioprocess Engineering, University College Dublin, Belfield, Dublin 4, Ireland

<sup>b</sup> Conway Institute of Biomolecular and Biomedical Research, University College Dublin, Belfield, Dublin 4, Ireland

<sup>c</sup> School of Medicine and Medical Science, University College Dublin, Belfield, Dublin 4, Ireland

<sup>d</sup> School of Electrical, Electronic and Mechanical Engineering, University College Dublin, Belfield, Dublin 4, Ireland

### ARTICLE INFO

#### Article history:

Received 24 February 2011

Received in revised form 26 April 2011

Accepted 13 July 2011

Available online xxxx

#### Keywords:

Biomaterial

Hydroxyapatite coating

CoBlast

Mesenchymal stem cells

Osteoconduction

Osseointegration

mRNA

PCR

### ABSTRACT

The novel non-thermal CoBlast process has been used recently to create a hydroxyapatite coating on metallic substrates with improved biological response compared to an uncoated implant. In this study, we compared the biological effect of coatings deposited by this process and the industrial standard technique – plasma-spray. Physicochemical properties of these two coatings have been found to be significantly different in that CoBlast HA is less rough but more hydrophilic than the plasma-spray HA as evidenced by data obtained from profilometry and goniometry. Mesenchymal stem cell attachment and adhesion are enhanced on CoBlast HA. Analysis by a combination of EDX and ICP suggests that the higher crystallinity retained by the CoBlast HA result in slower coating dissolution. Detailed *in vitro* evaluation reveals that plasma-spray HA might induce slightly faster cell proliferation and earlier osteogenic differentiation, but CoBlast HA becomes equivalent to it by the late osteogenic stage. PCR array facilitated the identification of differentially regulated genes involved in various functional aspects of *in vitro* osteogenesis by the CoBlast HA coating. The expression level of the functional protein products of these genes are in agreement with the PCR data. Coating metallic screws with HA significantly improves the *in vivo* osseointegration. By measuring of removal force using torque measurement instrument and analyzing the patterns found in X-ray images it is demonstrated that the two HA coatings elicit comparable osseointegration. Using simulated impaction model, CoBlast HA is shown to maintain better performance in cell attachment and mineralization than plasma-spray HA, especially following significant impactions. This might indicate a potentially greater osteoconductivity of CoBlast HA coating in shear-stress associated surgical applications. Collectively, it was demonstrated that CoBlast HA is an effective alternative to plasma-spray HA coating and a promising replacement for specialized surgical applications.

© 2011 Elsevier Inc. All rights reserved.

### 1. Introduction

Hydroxyapatite (HA), being chemically similar to the inorganic component of bone mineral, is one of the most popularly used bioactive ceramics in the surgical repair of hard tissue trauma and disease (Paital and Dahotre, 2009). HA's successful applications have been witnessed in a range of surgical specialties: bone substitute in bony defects restoration in orthopaedic surgery (Koshino et al., 2001), sinus obliteration (Moeller et al., 2010) and ossicular chain reconstruction (Pasha et al., 2000) in otolaryngological surgery, as well as craniofacial augmentation in plastic surgery (Quatela and Chow, 2008). In addition, HA has been extensively used as a thin film coating on titanium (Ti) alloys in load-bearing scenarios (Jaffe and Scott,

1996) and shear stress-susceptible applications (Sandén et al., 2002). The underlying rationale is to combine the high strength/weight ratio of the metallic alloy and the osteoconductivity and dissolubility of HA to achieve improved osseointegration. The outcome would be accelerated fixation of the implant by the adjacent newly formed bone tissue (Landor et al., 2007). Although various well-studied techniques exist to deposit HA onto Ti alloy substrate, plasma thermal spraying has been the industrial benchmark process owing to its high deposition rate, good biocorrosion resistance and substrate fatigue resistance of the coating, and capability to obtain various coating thickness (Sun et al., 2001). Nevertheless, the high thermal energy utilized in the plasma-spray process is its main drawback as described in the following series of events: (1) inevitable and unadjustable precipitation of crystal phases such as tricalcium phosphate (TCP) and tetracalcium phosphate (TTCP), (2) decreased crystallinity resulted in increased solubility of the coating, and (3) separation of the coating and possibly unsatisfactory *in vivo* bone fixation (Sun et al., 2003; Xue et al., 2004). Furthermore, the high temperature encountered

\* Corresponding author at: School of Chemical and Bioprocess Engineering, University College Dublin, Belfield, Dublin 4, Ireland. Tel.: +353 1 7161862; fax: +353 1 716 1177.

E-mail address: [m.al-rubeai@ucd.ie](mailto:m.al-rubeai@ucd.ie) (M. Al-Rubeai).

eliminates the possibility of simultaneous deposition of protein or peptide based drugs such as antibiotics, anti-inflammatories and osteoinductive growth factors (Kazemzadeh-Narbat et al., 2010; Leonor et al., 2009).

Recently, an innovative room temperature microblasting coating process, namely CoBlast™, has been reported (O'Neill et al., 2009) and gained many interests by virtue of its promising performance during *in vitro* osteoconduction and *in vivo* osseointegration (O'Hare et al., 2010). CoBlast's technical versatility also allows improvement on the resultant coating's bioactivity by means of altering dopant and/or abrasive. A successful model is the creation of HA/bioglass composite coating by incorporating another extraordinary bioceramic-45S5 Bioglass (Tan et al., 2011). However, there has been no direct comparison between the HA coatings produced by this novel technique and the conventional plasma-spray technique. Therefore, one of the objectives of this study is to comprehensively compare the material properties, *in vitro* osteoconductivities and *in vivo* osseointegration on as-received HA coatings. Human mesenchymal stem cells (MSCs) have been chosen as the *in vitro* cellular model based for two reasons: (1) the bone marrow cavity, where HA coated femoral implant is inserted during total hip replacement, contains abundant pluripotent MSCs that is an unlimited self-renewal source to differentiate into osteoblastic cells (Bilezikian et al., 2008; Compston, 2002), (2) MSCs and HA-MSCs complex have already exhibited promising clinical potential in regenerative medicine (Adachi et al., 2005; Barry and Murphy, 2004). Understanding the interaction between MSCs and the HA coating is crucial, especially by bridging the cellular and mRNA levels in a pathway-specific pattern. Thus, we connected results from cell attachment/adhesion, osteogenic differentiation and PCR array with the material difference between the two HA coatings.

As mentioned above, HA coating's main usage is in load-bearing surgical applications such as the acetabular and femoral prosthesis in a total hip replacement (THR) which can be accomplished in two approaches: cemented and cementless. The surgical technique applied in cementless THR to insert and fix the implant is called 'press-fit' during which impact forces are generally employed (Canale and Beaty, 2007). A HA coating that is less vulnerable to damage from impaction or shear stress would undoubtedly persevere longer *in situ* leading to the improved outcome of implantation. Cracking and delamination are not uncommon even in as-received and physiological fluid treated plasma-spray HA coatings (Lynn and DuQuesnay, 2002; Sun et al., 2003), but very little is known whether impaction or shear stress would worsen these features. Based on the morphological and physicochemical differences between the two as-received HA coatings, we hypothesized that their responses to the impaction would be different. Hence the second objective of our study is to answer a clinically relevant question: whether and how does physical impaction have an effect on the osteoconductivity of the HA coatings. In order to reproduce the 'hammering' commonly applied in cementless THR, we developed a simulated impaction system consisting of clamping and free-falling components. Changes in osteoconductivity by increasing number of impaction up to 16 times were analyzed in terms of cell attachment, osteogenic differentiation and *in vitro* matrix mineralization.

## 2. Materials and methods

### 2.1. Hydroxyapatite coatings deposition

HA coatings on Grade V Ti–6Al–4V alloy substrates were achieved on 20 mm × 20 mm × 1 mm coupons (Lisnabrin Engineering Ltd., Cork, Ireland) for *in vitro* examinations and on φ2.7 mm × 10 mm self-tapping cortex screws (Syntec Scientific Corporation, Taiwan) for *in vivo* study respectively. The *Ra* of the Ti alloy coupons were  $0.32 \pm 0.02 \mu\text{m}$  measured by optical profilometry based on 8 readings. All

samples underwent pre-deposition processes including mechanical polishing, immersing in methanol and acetone, as well as brief ultrasonic cleaning.

Thereafter CoBlast (EnBIO, Cork, Ireland) HA coatings were deposited in a system shown schematically in Fig. 1. In brief, dopant – HA (S.A.I., Vaulx-en-Velin, France) and abrasive – MCD (Himed, New York, USA) were supplied by corresponding powder feeders and simultaneously blasted through separate nozzles onto metallic substrates. The essential deposition parameters including particle size, nozzle angle and height, powder feeder pressure and deposition direction are clearly illustrated in Fig. 1. All samples underwent post-deposition cleaning by blasts with clean dry air at 60 psi to remove non-adhered particles. They were then stored in a desiccator until autoclaved at 121 °C for 20 min prior to experiments.

On the other hand, plasma-sprayed HA coatings were attained on the same Ti alloy coupons and screws from APS Materials Inc. (Waterford, Ireland). The up-to-date APS master file conforms to the FDA guidance document titled '510(K) Information needed for hydroxyapatite coated orthopaedic implants'. In short, samples underwent grit blasting, substrate cleaning, HA plasma spray and removal of overspray.

### 2.2. Coating characterizations

Optical profilometry (Wyko NT1100, Veeco, Cambridge, UK) was conducted on the surfaces to obtain two fundamental surface roughness values (*Ra* and *Rz*). Hydrophilicity, expressed as water

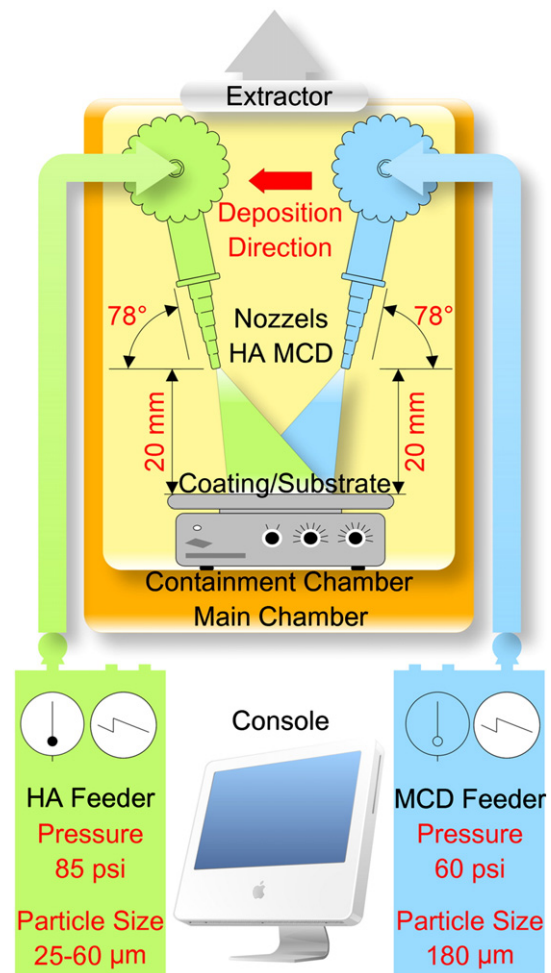


Fig. 1. Schematic of CoBlast deposition system. Black texts represent the core components of the system, and red texts refer to the essential parameters used to acquire HA coatings.

contact angle, was measured via the sessile drop method using a computer automated goniometer (OCA 20, Dataphysics, Filderstadt, Germany). Two locations were chosen on each sample, and 4 samples were examined. Thus, there were in total eight replicates for each result. HA surfaces were coated with gold by a turbo pumped high-resolution sputter coater (K575X, EmiTech, Kent, UK) before being examined qualitatively under scanning electron microscope (SEM, Quanta 3D FEG, FEI Ltd., Hillsboro, US) which operated at 5 kV and 5.92 pA with an observation angle at 45°. Coating thickness was quantified using a PosiTector 6000 Memory 3 thickness gauge (Defelsko, New York, US). Cross sectional images of coatings were acquired using a tabletop SEM (TM-1000, Hitachi, Berkshire, UK). Images were merged using Photoshop® CS5 Extended (Adobe, Dublin, Ireland).

X-ray photoelectron spectroscopy (XPS) analysis was performed using an Axis Ultra DLD spectrometer (Kratos Analytical, Kyoto, Japan) at an analysis chamber pressure of  $10^{-8}$  Torr. All samples were subjected to 5 min of Ar ion sputtering (2 keV) prior to analysis to remove the surface layers. A monochromated AlK $\alpha$  X-ray (1486.58 eV) source operating at a 10 mA current and an anode voltage of 15 kV was utilized. A charge neutralizer was used to compensate the charge build up on the insulating HA surfaces. C (1 s) peak at 284.8 eV was used as a charge reference to determine binding energies. Pass energy of 160 eV and 20 eV were employed for survey spectra and narrow regions respectively. CasaXPS version 2.3.15 software (CasaSoftware Ltd., Cheshire, UK) using Gaussian-Lorentzian line shapes and a Shirley background was employed to process the quantitative data from three locations of each sample, reported as average relative atomic % concentration (At%).

Energy dispersive X-ray (EDX) analysis was carried out using an EDX Apollo XV Silicon Drift detector (EDAX Inc., Mahwah, USA) in conjunction with the SEM as previously stated. EDX mapping was subsequently conducted for HA coatings that sustained impactions. All the samples for EDX analysis were native interfaces used without the application of a conductive thin-film coating.

Ca<sup>2+</sup> ion release from the two types of HA coatings into cell growth medium (composition described in next section) was monitored over a 5-week period using inductively coupled plasma optical emission spectroscopy (ICP-OES, Vista-MPX, Varian, Oxford, UK). In brief, dissolution samples were digested in nitric acid prior to the argon plasma treatment. The excitation and emission radiation were measured sequentially at predetermined ionic line wavelengths and was then compared with the intensities obtained from standard solutions. This was conducted on 6 separate samples.

### 2.3. Mesenchymal stem cell culture conditions

Human mesenchymal stem cells (MSCs) were obtained commercially from ScienCell™ Research Laboratories (California, USA) and used for all *in vitro* experiments. They were isolated from human bone marrow, cryopreserved at passage one culture and delivered frozen. Subsequent culture conditions were as follows: 37 °C in a humidified 5% CO<sub>2</sub> atmosphere in a growth medium containing 88% (v/v) Dulbecco's modified Eagle's medium (DMEM), 10% fetal bovine serum, 1% L-glutamine and 1% Penicillin/Streptomycin. All reagents above were from Sigma-Aldrich (Dorset, UK). Cells were sub-cultured every 2 days at 80% confluency, and passages 5 to 8 were used. All cellular studies were performed in 6-well tissue-culture plate (Sarstedt, Wexford, Ireland) where each coupon was immersed by 3 ml growth medium. Prior to inoculation onto coupons, MSCs were washed twice with pre-warmed Dulbecco's phosphate buffered saline (DPBS), detached with Accutase (both from Sigma-Aldrich), mixed immediately with equivalent volume of growth medium, centrifuged at 280 RCF for 5 min, and collected. Osteoblastic differentiation of MSCs were induced by supplementing growth medium with 10 nM dexamethasone, 0.1 mM L-ascorbic acid and 10 mM  $\beta$ -glycerophosphate.

Both growth medium and osteogenic medium were refreshed twice a week.

### 2.4. Cell attachment and cell adhesion

Relative cell attachment was determined using a colorimetric approach. MSCs were seeded onto the surface at a concentration of  $6 \times 10^5$  cells/ml in growth medium. This relatively high concentration was used to saturate the bonding capacity of each surface to prevent falsely low results. None of the surfaces underwent any pre-conditioning with serum or growth medium. Cells were allowed to settle down completely until 12 h later when preparation procedure for SEM was initiated. At this time point, samples were gently washed twice with DPBS and moved to new 6-well tissue culture plates. 3 ml of 0.2% (w/v) crystal violet in 10% ethanol was added to each well to simultaneously fix and stain the cells. After incubation for 5 min at room temperature, stain was removed by gentle washing with DPBS three times. Then 3 ml of solubilization buffer (1:1 mixture of 0.1 M NaH<sub>2</sub>PO<sub>4</sub>, pH 4.5 and 50% ethanol) was added, incubated for 5 min and gently shaken until the cell-bound stain was completely solubilized. 100  $\mu$ l of the homogenized supernatants were placed in triplicate into a 96-well plate, and the absorbance read on a microplate reader (GENios™, TECAN, Reading, UK) at 570 nm. The absorbance value was subtracted by the background reading from corresponding acellular samples. This was to eliminate the interference from the highly absorbent plasma-spray HA coating.

Attached cells from the other replicate were fixed *in situ* with 2.5% (w/v) glutaraldehyde for 30 min at 4 °C followed by dehydrating with a series of ethanol/H<sub>2</sub>O solutions. These solutions increased in both ethanol concentration (50%, 75%, 90%, 95% and 100%) and reaction time (10 min, 10 min, 15 min, 20 min and 30 min). Samples were finally treated with 3 ml hexamethyldisilazane (HMDS) for 1 min, left to air dry at room temperature and stored in a desiccator. SEM observation was carried out following same steps as previously described.

Cell adhesion was measured indirectly by quantitative data from cell detachment assay. Cells were inoculated in the same way introduced in cell attachment experiment, except that they were allowed to attach for 24 h during the transition between cell attachment and cell proliferation. Attached cell number was determined by the alamarBlue® assay (Invitrogen, Paisley, UK) which is an *in situ*, non-toxic metabolic assay (Tierney et al., 2009). In brief, 10% (v/v) alamarBlue® reagent was aseptically added to cells in existing media and incubated at 37 °C for 3 h. The absorbance of the resultant medium was measured colorimetrically at 570 nm normalized to 600 nm. Cell number was calculated based on a standard curve. Following this step, cells were washed with DPBS, detached by Accutase, carefully collected. Cell viability and count were obtained through Cell Lab Quanta™ SC flow cytometry system (Beckman Coulter Inc., Florida, US) which utilized propidium iodide as a fluorescent DNA dye. Data were reported as % of detached cells = detached cell number / attached cell number prior to detachment. Cell viability was over 95% at the end of Accutase detachment.

### 2.5. Cell proliferation and osteogenic differentiation

Cells were seeded onto the surface at a density of  $6 \times 10^4$  cells/ml. This relatively low concentration was intended to prevent the cells from reaching confluency too soon. After 24 h, the samples were gently washed twice with DPBS and moved to new 6-well tissue culture plate so that the cells accounted for later experiments were only those attached to coupons rather than those originally attached to the plastic bottom of the wells. The growth medium was refreshed every two days. After 1, 3 and 5 days, cells were fully collected and the number determined by flow cytometry.

Osteogenic medium was introduced on day 7 after cells became entirely confluent, and changed once every two days to minimize the instability of L-ascorbic acid in neutral pH. On day 15, the supernatant and cell layer from the same well were analyzed to quantify osteocalcin (OC) and alkaline phosphatase (ALP) (EC 3.1.3.1) respectively. ALP is expressed mainly intracellularly, and OC are primarily secreted into the supernatant, thus their results were normalized to intracellular total protein content and total cell number respectively. The cell layer was lysed and extracted protein was solubilized by a cell lysis/extraction reagent (CellLytic™ M, Sigma-Aldrich) on a gyratory rocker (Stuart® SSL3, Essex, UK). SensoLyte® ALP assay kit (AnaSpec, Cambridge, US) was employed to detect ALP concentration. Upon dephosphorylated by ALP, *p*-Nitrophenyl phosphate (pNPP) turned yellow and its color change was directly proportional to ALP (Morris et al., 1992). This colorimetric assay was finished by detecting the absorbance at 405 nm. The total intracellular protein content was quantified using a bicinchoninic acid (BCA) protein assay kit (Sigma-Aldrich) in accordance with supplier's instructions. The production of OC in supernatants was determined colorimetrically using an immunoenzymatic assay (Invitrogen) employing highly specific monoclonal antibodies and horseradish peroxidase-labeled OC. The total cell number was pre-determined using alamarBlue assay as above.

## 2.6. Reverse transcription PCR (RT-PCR)

At the end of each time-course, RNeasy® Plus Mini kit (QIAGEN, West Sussex, UK) was used to extract and purify RNA from collected cells without the need for additional DNase digestion. In general, cells were lysed with CellLytic M and disrupted with a homogenizer. Then the lysates were passed through a genomic DNA (gDNA) eliminator spin column, ethanol was added to bind total RNA, mixture was transferred to an RNeasy spin column, and RNase-free H<sub>2</sub>O was added to elute RNA. The purity and integrity of total RNA was checked by NanoDrop™ spectrophotometer (ND-1000, Thermo Scientific, Surrey, UK) and Agilent 2100 Bioanalyzer in conjunction with RNA 6000 Nano chip (Agilent Technologies, Cork, Ireland), respectively. First-strand complementary DNA (cDNA) was synthesized by using the RT<sup>2</sup> PCR array First Strand Kit (SABiosciences Corporation, Frederick, USA). The RT-PCR cycling conditions were as follows: the RT 'cocktail' was incubated at 42 °C for exactly 15 min and immediately stopped by heating at 95 °C for 5 min, and 91 µl of H<sub>2</sub>O was then added to each 20 µl cDNA synthesis reaction.

## 2.7. Real-time PCR (Q-PCR) array analysis

Osteogenesis pathway-specific PCR array system (SABiosciences Corporation, Frederick, USA), designed to combine the microarray profiling capabilities with Q-PCR performance, was employed to screen 84 genes that are related to osteogenic differentiation. A 96-well plate with 10 µl reaction mixtures per well containing cDNA and SYBR Green/ROX based PCR master mix was used in 7900HT Fast Real-Time PCR System (Applied Biosystems, Cheshire, UK). A two-step cycling program (1 cycle of 10 min at 95 °C for enzyme activation, followed by 40 cycles of 15 s at 95 °C for denaturation, and 1 min at 60 °C for annealing and extension) was used. In order to obtain statistically robust data, we analyzed each sample in triplicate. The critical threshold (CT) values of 84 target genes and 5 housekeeping genes (*B2M*, *HPRT1*, *RPL13A*, *GAPDH* and *ACTB*) were imported into RT<sup>2</sup> Profiler PCR Array Data Analysis Software version 3.3 (SABiosciences Corporation). It converted CT values into fold-change between CoBlast HA and plasma-spray HA samples based on the  $2^{-\Delta\Delta CT}$  method as previously described (Livak and Schmittgen, 2001). T-test was used for statistical comparison of the mean CT values derived from the triplicates of each HA sample (Yuan et al., 2006). A fold up- or down-

regulation of >2 or <-2, as well as *P*-value of <0.05 were chosen as the criteria for significantly altered gene expression.

## 2.8. Enzyme-linked immunosorbent assay (ELISA)

In order to accurately verify the results of PCR array functional protein expression level, we conducted sandwich ELISA on few proteins that were translated from mRNAs and whose expression was significantly altered. Six replicates of coatings were used to achieve statistical sample size. The ELISA was accomplished using DuoSet® ELISA development system (R&D Systems, Abingdon, UK) in a supplier-instructed method: analytes or standards were sandwiched and immobilized by capture antibodies and detection antibodies. Streptavidin-HRP was added to bind to the detection antibody, followed by the addition of tetramethylbenzidine (TMB) substrate solution. The developed blue color was in proportion to the amount of analytes present in the sample, and it was converted into yellow whose absorbance was measured at 450 nm.

## 2.9. In vivo testing of osseointegration

Local ethical regulation was complied with throughout the animal trial. A transcortex femoral implantation procedure was conducted using skeletally mature male New Zealand rabbits (O'Hare et al., 2010). They were housed and acclimated for 2 weeks before the surgery. The age and weight range of the experimented rabbits immediately before implantation were 12 ± 1 month old and 2.94 ± 0.28 kg, respectively. HA-coated and uncoated φ2.7 mm × 10 mm self-tapping cortex screws (Syntec) were randomized so that no one kind would be implanted in the same femur. Ten rabbits were implanted with screws with two screws on each femur in order to ensure that each coating type had at least 10 replicates prior to sacrifice.

The rabbits were anaesthetized using pentobarbital 30 mg/kg intravenously. The anterolateral surface of the femur just distal to the level of lesser and third trochanter was exposed sufficiently through layers: skin, subcutaneous tissue, tensor fasciae latae, and intermuscular junction between vastuslateralis and biceps femoris. Two adjacent transcortex 2 mm diameter holes were drilled using sterile saline site flooding as the drill bit and bone site coolant during drilling. A hand held 2.5 mm Allen key was used to acquire a bite on the threads of the self-tapping screw in the cortical bone. Then a MTS 858 torque wrench (MTS System, Minneapolis, USA) was employed to further insert the screws stopping at an insertion torque load of 0.07 Nm which usually corresponds to the tip of screw locating on the opposing endosteal surface of the femur and tightening up (Fig. 8B). Wound was closed in layers: fascia sutured with 5-0 Vicryl, and skin sutured with 4-0 Ethilon (both from Ethicon Inc., Shanghai, China). All rabbits received post-operative analgesics and antibiotics. Eight weeks after the implantation, rabbits were sacrificed and femurs exposed for biomechanical testing. The same handheld torque gage used during screw insertion was applied as a screwdriver with its tip connected to the screw head. The maximum force encountered during untightening the screws was recorded and displayed on the built-in force meter. Three blinded independent radiologists analyzed the X-ray images and a consensus was reached in terms of which X-ray images were representative of each coating type.

## 2.10. Impaction test model for in vitro osteoconductivity analysis

Freshly harvested bovine cortical bone close to proximal femur was cut by band-saw (WBS 20L, Brisbane Saw Service, Brisbane, Australia) into blocks. They were visually checked to exclude samples with defects or growth plates, cleaned with ethanol and copious H<sub>2</sub>O, and finally randomized for impaction. The impact force was pre-determined (Mushipe et al., 2006) by recording and averaging the

surgeons' forces in hammering femoral component. This was then simulated into an apparatus (Fig. 2) consisting of a dropping 1.5 kg steel cylinder from a height of 0.88 m. The test HA samples were impacted 5 and 10 times, cleaned with air blast and brief IPA sonication, and stored with unimpacted HA samples in a desiccator until autoclave before *in vitro* cellular experiments.

### 2.11. Matrix mineralization and Alizarin red staining

Alizarin red staining was used to determine bone nodule formation and matrix mineralization which is a crucial *in vitro* stage towards the formation of calcified extracellular matrix associated with true bone. MSCs were inoculated at of  $3 \times 10^5$  cells/ml and cultured on impacted HA samples in the presence of osteogenic medium for up to 21 days. For qualitative probe, cells were fixed in ice-cold 70% ethanol or 1 h at room temperature, rinsed with excess dl H<sub>2</sub>O, stained with 40 mM Alizarin Red solution (Sigma-Aldrich) at room temperature for 5 min, and washed copiously prior to visualization under a stereo microscope (SZX12, Olympus, Essex, UK). For quantitative assessment, calcified nodules were first trypsinised from the colonized HA surface and then fixed and stained (Gough et al., 2004). This was carried out to avoid interference from calcium-containing substrate material. The Alizarin dye was then extracted, neutralized, and colorimetrically detected at 405 nm (Gregory et al., 2004).

### 2.12. Statistical analysis

Results were analyzed using Student's *t*-test with  $\geq 5$  independent samples. Data is expressed as mean  $\pm$  standard deviation. *P* value < 0.05 was considered significant. All statistical calculations were implemented using SPSS Statistics 19 (IBM®, Chicago, IL). An asterisk is labeled above the error bar of CoBlast in figures where there is statistical difference between CoBlast and plasma-spray HA coatings.

## 3. Results and discussion

### 3.1. Surface analysis of the coatings

Surface roughness and hydrophilicity were measured by optical profilometry and water goniometry, respectively. Compared to plasma-spray HA, CoBlast HA is significantly smoother (Fig. 3A) as evidenced by lower *Ra* and *Rz* (*P* < 0.01). The values here are consistent

with our previous findings (Tan et al., 2011) which also showed the versatility of CoBlast process in altering surface roughness by simply using various abrasive/dopant combinations. In addition, CoBlast HA is more hydrophilic as indicated by a lower water contact angle (*P* < 0.001). This is most likely due to the high kinetic energy induced in the substrate surface disruption by the impinging HA (O'Neill et al., 2009).

SEM images reveal apparent similarities and dissimilarities in the surface morphology. Plasma-spray HA presents with intrinsic features of thermal spraying: partially melted large and fine particles, spheroidized particle, flattened splat, and accumulated splat

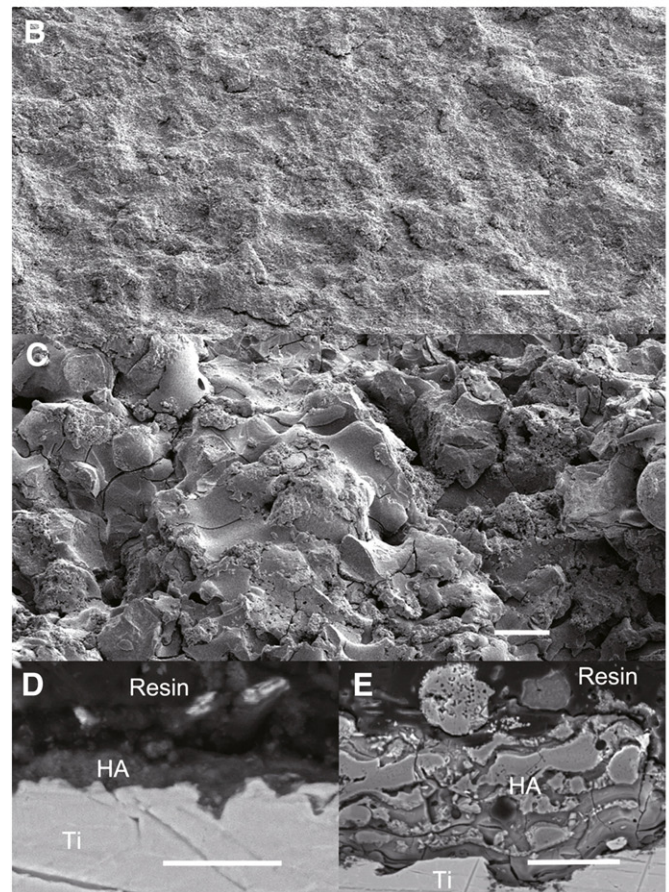
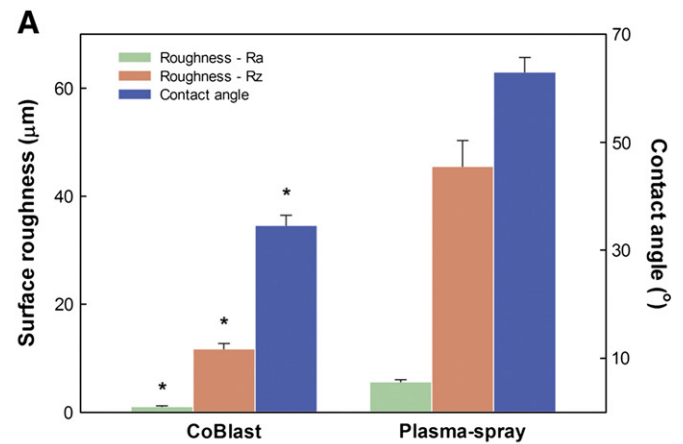


**Fig. 3.** Essential material characteristics of the HA coatings. **A:** Surface roughness and water contact angle. **B–E:** SEM images of as-received HA coatings. **B:** Surface of CoBlast HA coating. **C:** Surface of Plasma-spray HA coating. **D:** Cross section of CoBlast HA coating. **E:** Cross section of Plasma-spray HA coating. Scale bar = 20 µm. (HA = hydroxyapatite, Ti = titanium alloy substrate).

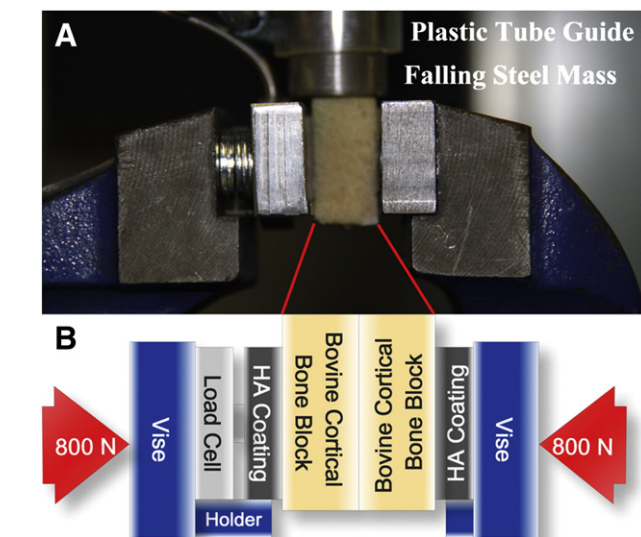


**Fig. 2.** Illustration of the impactation system for the *in vitro* osteoconductivity analysis. **A:** Photograph of the impactation system. **B:** Schematic of the impactation system.

(Fig. 3C). None of these are observed on CoBlast HA surface due to its non-thermal nature (Fig. 3B). Apart from these morphological differences, both HA coatings have hairline fractures on the surface, except that CoBlast HA's cracks are less dense and noticeable. In order to explore the extent of these fine fractures, cross sectional SEM images were acquired. The delicate crevices appear to be completely superficial in CoBlast HA coating (Fig. 3D), which is an opposite scenario to those in the plasma-spray HA coating where the majority of the surface cracks extend into the deeper layers of the coating even penetrating to the Ti substrate (Fig. 3E). The cause of this feature is the dramatic and irregular cooling within a thick coating (Sun et al., 2003; Tsui et al., 1998) following deposition. When combined with the mismatch in cooling rates between the metallic substrate and HA, this could together result in coating delamination and detachment, especially in simulated body fluid (SBF) and *in vivo* (Clemens et al., 1999; Hayashi et al., 1994; Lynn and DuQuesnay, 2002). This is one of the reasons that we conducted the impaction study, as we would not expect this to be the case with the CoBlast HA coating which contains mechanical interlocking and tribochemical bond between the HA and the underlying metallic substrate (O'Hare et al., 2010). In view of these findings, the fine fractures on the HA coating surface is more than likely caused by unimpregnated HA particles loosely and partially attached to underlying mature HA coating, as these cracks tend to disappear after simple washing during cell handling (Fig. 5B). An additional piece of information from the cross sectional SEM image is the qualitative comparison of the coating thickness: plasma-spray HA is at least 3 times thicker than CoBlast HA. This is confirmed with the value from a depth device based on magnetic and eddy current principles (Fig. 4A): the CoBlast HA coating measures 8  $\mu\text{m}$  thick in average, whereas most plasma-spray HA coatings thickness falls into 30–40  $\mu\text{m}$  range ( $P < 0.001$ ).

Chemical composition of the HA coatings were quantified using XPS whose results are reported in Table 1. The pristine Ti–6Al–4V substrate exhibits an abundant titanium oxide layer with possibly either a hydrocarbon layer on top or carbon contamination from the passivation process. Both HA coatings present significant levels of Ca, P and O suggesting a robust formation of HA coating. Furthermore, both coatings have satisfactory coverage as no Ti is detected. In order to reliably reflect the atomic calcium to phosphorous ratio, EDX was performed. CoBlast HA coating is found to have a Ca/P ratio close to 1.67 which is the ratio in stoichiometric HA ( $\text{Ca}_{10}(\text{PO}_4)_6(\text{OH})_2$ ). This is ascribed to the preservation of HA crystallinity during non-thermal CoBlast processing. In contrast, plasma-spray HA coating's Ca/P ratio is around 1.9 ( $P < 0.05$ ) which reflects a mixture of thermal degradations of HA as previously discussed. It is broadly agreed that various crystalline forms of calcium phosphate present in plasma-spray HA coating generally follow such decreasing order in terms of their dissolution rate:  $\text{TTCP} > \alpha\text{TCP} > \beta\text{TCP} \gg \text{HA}$  (Hench and Wilson, 1993; Kokubo, 2008). As a consequence, the [Ca] in CoBlast culture, as manifested by the ICP-OES, maintained around 68 ppm which is the baseline concentration in cell growth medium (Fig. 4B). The cell culture medium used contains DMEM which is a modified form of SBF. A slight increase in dissolution rate of CoBlast HA is observable after 3 weeks of immersion. On the other hand, plasma-spray HA has a significantly faster coating dissolution compared to CoBlast HA in the first 2 weeks (~50 ppm/week) followed by a stabilization third week (~20 ppm/week). A reversal of the trend is noted after the fourth week when coating dissolution rate starts to decline steadily at a rate of 10 ppm/week (Fig. 4B). Similar trends have been reported, and the underlying mechanism is thought to be the increased ionic activity products of apatite leading to the increased consumption of Ca and P ions in the medium (Gross and Berndt, 1994; Kweh et al., 2002).

Almost all aspects of material properties are different for CoBlast and plasma-spray HA coatings. This is indicative of distinct nature of the two coating techniques. The most reliable reflection of the net result of this unlikeness would be the biological activity of these

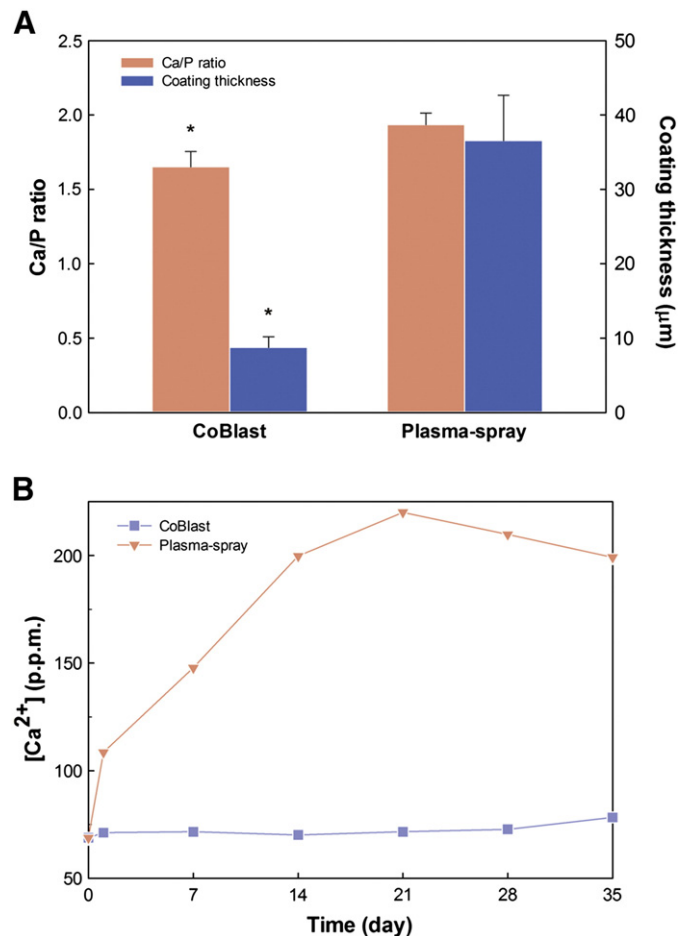


**Fig. 4.** Chemical properties of the HA coatings. **A:** The calcium to phosphorous atomic ratio of the two HA coatings obtained from EDX, and average coating thickness. **B:**  $\text{Ca}^{2+}$  ion dissolution from the two HA coatings in cell growth medium up to 5 weeks. The baseline  $[\text{Ca}^{2+}]$  in cell growth medium was measured and expressed at day 0.

coatings. Thus, all essential material characteristics discussed above will be associated independently or collectively with major aspects of *in vitro* osteoconduction and *in vivo* osseointegration of the HA coatings in the following sections.

### 3.2. Cell attachment and adhesion

Human MSCs were allowed to discern and attach to the HA coatings after 12 h of incubation. The absorbance values recorded from crystal violet assay demonstrate that the amount of attached cells on CoBlast HA is almost twice of that on plasma-spray HA ( $P < 0.001$ , Fig. 5A). This significant difference is reinforced by the distinct cell morphology visualized by SEM. The representative MSC can be hardly differentiated as the cellular edge is visually inseparable from the CoBlast HA coating (Fig. 5B), except for a single long cell process extending away from the cell body. The lamellipodia is so widely dispersed and thin that the underlying coating topography can be apparently revealed. In addition, there are numerous marginal

**Table 1**  
Quantitative XPS analysis of metallic substrate with and without HA coatings (Data is shown as atomic % elemental composition).

Surface	Ca	P	Ti	O	C
Ti–6Al–4V	2	4	13	45	36
CoBlast HA	16	11	–	55	18
Plasma-spray HA	19	9	–	52	20

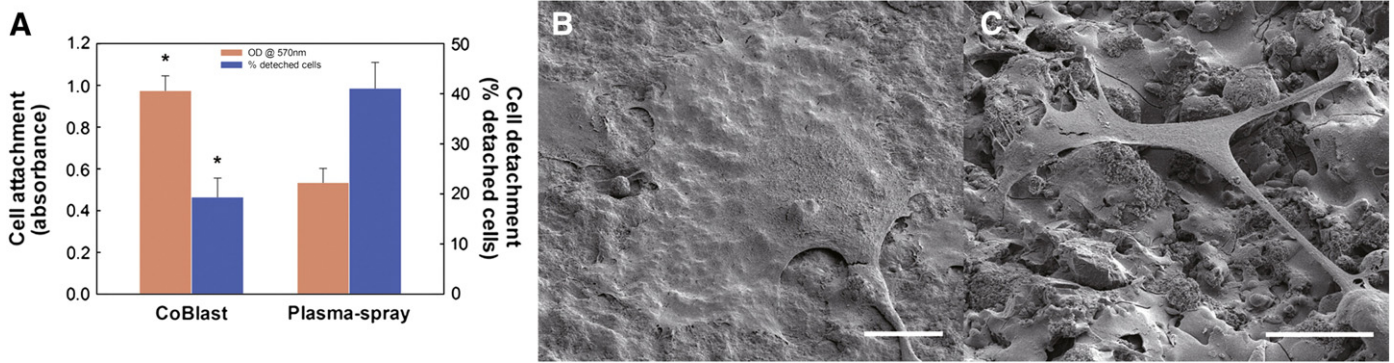


**Fig. 5.** Cell attachment and adhesion. **A:** Quantitative assessment of MSCs attachment 12 h after inoculation, and indirect measurement of cell adhesion 24 h after inoculation. **B:** SEM morphology of MSCs attached on CoBlast HA coating. **C:** SEM morphology of MSCs attached on plasma-spray HA coating. Scale bar = 30  $\mu$ m.

filopodia helping the cell to anchor itself to the coating. Considering the average diameter of MSCs in suspension before attachment is only  $7.8 \pm 2.6 \mu\text{m}$  (flow cytometric measurement), the cell surface area has increased drastically since the diagonal distance has increased at least 10 times after adherence. Furthermore, this type of morphology is universally expressed by adhered cells indicating a good homogeneity of the CoBlast HA coating. In comparison, MSC adhered to plasma-spray HA coating presents with a typical fibroblastic morphology similarly observed in MSCs cultured on a normal plastic tissue plate, even though the tissue culture plate is almost completely flat whereas plasma-spray HA has an  $R_z$  of nearly  $50 \mu\text{m}$ . The consequence of this is that MSC is attached to plasma-spray HA only through scanty adhesion points located at the tip of the multiple long cellular processes. The majority of the remaining part of the cell, including cell body and cell process stem, is rather suspended from the surface (Fig. 5C). This most likely explains why cell adhesion is also stronger on CoBlast HA coating (Fig. 5A). Using Accutase, only 20% of the adherent cells are detached from CoBlast coating, whereas twice as many cells are detached from plasma-spray coating.

The generally superior cell attachment, morphology and adhesion on CoBlast HA coating compared to plasma-spray most likely result from the distinct surface roughness and hydrophilicity as mentioned previously, as both parameters have profound influence on initial cell-material interaction (Paital and Dahotre, 2009). Most researchers in this field agree that surface energy/wettability has a positive relationship with cell adhesion events: the higher the hydrophilicity, the better the cell attachment (Lim et al., 2008; Liu et al., 2007; Paital and Dahotre, 2009; Redey et al., 2000). On the other hand, higher surface roughness should provide bigger surface area thus allow more cells to be attached. However, this rule seems to only apply to certain roughness range (Ponsonnet et al., 2003). We hypothesize this to be the case for plasma-spray HA coating as the topographical change from steep peak and deep trough (supported by relatively large  $R_z$ ) might be too dramatic for proper attachment of cells. This will be further validated in the impaction study.

### 3.3. Cell proliferation and osteogenic differentiation

Cell proliferation (Fig. 6A) demonstrated by the flow cytometric cell count displays a higher cell number ( $P < 0.05$ ) on CoBlast HA coating up to 3 days of culture, owing to better cell attachment for the first 24 h. This small but significant difference between the two HA coatings disappear at day 5. A valid explanation is that the greater ion concentration (e.g. Ca or P) in the plasma-spray culture from ICP results (Fig. 4B) could be beneficial for cell proliferation (Sun et al., 2007, 2009). Since the total cell number in a culture is the net result of cell mitosis and apoptosis, flow cytometry analysis on cell cycle distribution needs to be conducted in future work to ascertain true proliferation rate.

A distinguishing feature that defines MSCs is their multilineage differentiation potential, one of those cell lines being osteoblasts. We transformed MSC culture into osteogenic one on day 7 when cell confluency is same on both HA coatings. Standard osteogenic markers, such as ALP and OC, were quantified and normalized on day 15 (Fig. 6B). Cells grown on plasma-spray HA appears to have entered osteogenic phase earlier than those on CoBlast, as they express higher level of ALP ( $P < 0.05$ ) which is an early marker of ossification (Bilezikian et al., 2008). This rapid osteogenicity could well be due to plasma-spray HA's residual effect of faster coating dissolution. Interestingly, both HA cultures seem to have equivalent OC expression ( $P > 0.05$ ). Since OC level has a unimodal time distribution (Setzer et al., 2009), the seemingly comparable OC production could indicate either same or retarded stage

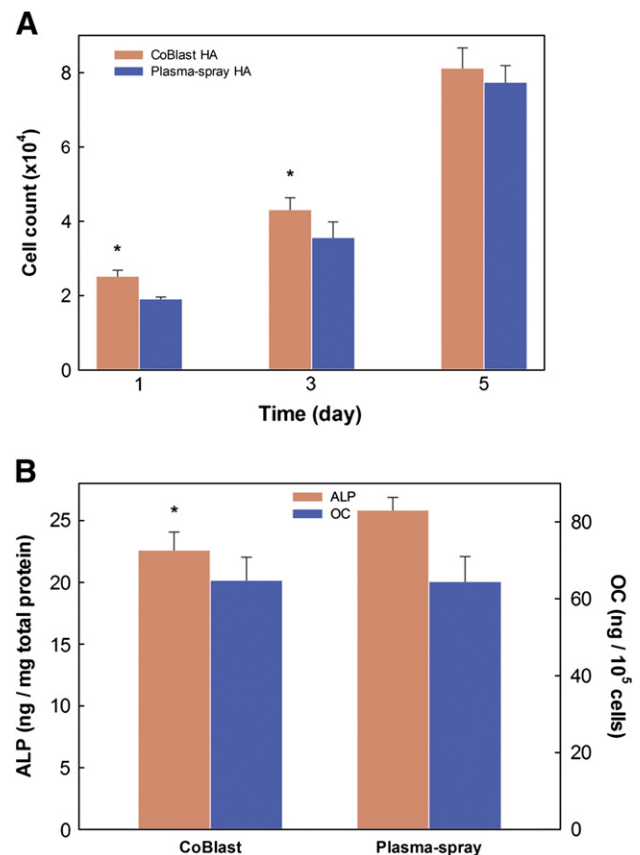


**Fig. 6.** Cell proliferation and differentiation. **A:** MSCs proliferation during 5 days culture. **B:** Osteogenic differentiation of MSCs, expressed as specific markers' levels. (ALP = alkaline phosphatase, OC = osteocalcin).

of osteogenesis. The exact temporal stage will be validated by the subsequent *in vivo* study.

### 3.4. Osteogenesis pathway gene and protein expression

Baseline osteogenic markers quantification is valuable in confirming the osteogenic differentiation potential of MSCs on HA coatings, but is insufficient in revealing the underlying complexity of osteogenic pathway. In view of this, PCR array combined with ELISA were conducted to supply in-depth information at mRNA and protein levels respectively. Among the focused panel of 84 genes related to osteogenic differentiation, CoBlast (vs. plasma-spray) results in the up-regulation of 3 genes while 4 genes are down-regulated (Table 2) at day 15. However, at day 25 only one gene was up-regulated and 2 genes down-regulated. These deregulated genes belong to 5 functioning gene groups which cover almost all aspects in osteogenesis development. The fact that there are more genes differentially regulated on day 25 than on day 15 suggests that the osteogenic potentials of the two HA coatings are becoming comparable while approaching the terminal stage of *in vitro* mineralization. The up-regulated genes are mainly involved in cell adhesion, whereas the down-regulated genes are essentially for cell growth. This is consistent with the cell adhesion and proliferation results, consolidating the connection between mRNA expression and cell behavior.

Unlike the data from traditional microarray analysis that usually needs to be confirmed at the transcriptional level by real-time PCR, our data obtained from RT<sup>2</sup> Profiler PCR array are genuine real-time PCR results. In authors' opinion, the most appropriate validation method should be at the translational level. We selected one deregulated gene from each functional gene group, and measured the expression of proteins translated from these mRNAs by using ELISA rather than western blotting which is a semi-quantitative approach. Results in Fig. 7 are broadly consistent with those from PCR array thus consolidating the reliability of this method. Proteins assayed by ELISA included VCAM1 which is a crucial cell-cell adhesion molecule for osteoblasts. It does not only function as intercellular glue but also as a transduce activation signal for bone metabolism (Tanaka et al., 1995). Another protein of interest is IGF1 which has been found

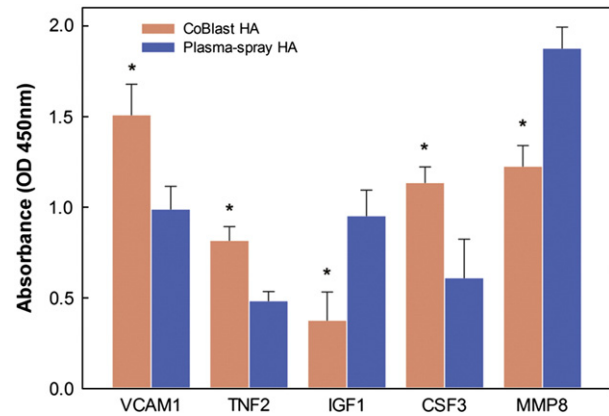


Fig. 7. ELISA of protein products translated from selected genes that had deregulation from osteogenesis specific pathway of MSCs grown on two HA coatings. (VCAM1 = vascular cell adhesion molecule 1, TNF2 = tumor necrosis factor 2, IGF1 = insulin growth factor 1, CSF3 = colony stimulating factor 3, MMP8 = matrix metalloproteinase 8).

to stimulate osteoblasts proliferation and ALP activity, and can be used as a therapeutic coating with HA to enhance its osteoconductivity (Zamboni et al., 1999). The ELISA results concur with previous cellular data in describing a scenario in which CoBlast HA induces superior cell attachment and adhesion whereas plasma-spray HA possibly evoke faster cell proliferation. However, an overall conclusion of these growth factors expression should be made judiciously as some of their interactions are still unclear (Bilezikian et al., 2008).

### 3.5. *In vivo* osseointegration

Transcortical self-tapping screws with or without HA coatings were inserted into rabbit femurs to test *in vivo* osseointegration which was analyzed both qualitatively and quantitatively. The histology work has been performed and reported recently on CoBlast samples (O'Hare et al., 2010). In order to consolidate previous *in vivo* work and avoid repetition, the osseointegration is evaluated macroscopically in this study. The immediate post-operative X-ray image (Fig. 8B) clearly displays the position of the screw: completely penetrate through one cortex with the screw tip in close proximity to the other. The subcutaneous shadow represents surgical emphysema which is one of the commonest complications. In addition, there is no sign of iatrogenic fracture or acetabulofemoral joint dislocation. The extent of osseointegration is quantified directly by measuring mechanical torque force while the screws are being removed. Coating Ti screws with HA significantly improves the osseointegration, as manifested by the higher torque out force ( $P < 0.01$ ) required to remove CoBlast and plasma-spray HA coated screws (Fig. 8A) compared to uncoated screws. However, there is no statistical difference in the resistance during removal between the two HA coated screws ( $P > 0.05$ ), indicating their similar osseointegration. No wound dehiscence or abscess formation was found in rabbits from which the screws were retrieved. A phenomenon worth mentioning is that prior to screw removal, very small amount of HA coating debris was found adjacent to the insertion site in 3 out of 40 cases. This coating debris is only found in the plasma-spray HA group. In all likelihood this is caused by coating delamination or detachment during screw insertion, followed by gradual decomposition of the loosened coatings *in situ*. It probably also explains the larger error bar/standard deviation of the torque out force recorded in plasma-spray group compared to other two groups (Fig. 8A). This is not surprising as the commonest host response to these particles would be to isolate and reject them, to the point of forming soft tissue fibrosis (Hench and Wilson, 1993; Lynn and DuQuesnay, 2002; Park, 2008).

Table 2

Genes deregulated in the osteogenesis pathway of human MSCs grown on CoBlast and plasma-spray HA coatings (CoBlast vs. plasma-spray on day 15 and 25 of osteogenic culture).

Functional gene grouping	Gene symbol (gene product)	GenBank ID	CoBlast vs. plasma-spray	
			p-Value	Fold change
<i>Day 15 in osteogenic culture</i>				
Cell adhesion molecules	<i>itgam</i> (Integrin, alpha M)	NM_000632	0.005	2.59
	<i>vcam1</i> (Vascular cell adhesion molecule 1)	NM_000088	0.017	3.16
Transcription factors	<i>tnf2</i> (tumor necrosis factor 2)	NM_004348	0.023	2.78
Cell growth and differentiation	<i>fgf3</i> (Fibroblast growth factor 3)	NM_005247	0.004	-2.06
	<i>igf1</i> (Insulin-like growth factor 1)	NM_000618	0.011	-2.17
ECM molecules, bone mineral metabolism	<i>col1a1</i> (Collagetype I, alpha 1)	NM_000088	0.027	-2.24
	Ossification <i>alpl</i> (Alkaline phosphatase)	NM_000478	0.015	-2.01
<i>Day 25 in osteogenic culture</i>				
ECM molecules, bone mineral metabolism	<i>Csf3</i> (colony stimulating factor 3)	NM_001711	0.001	3.66
	<i>bglap</i> (Bone gamma-carboxyglutamateprotein)	NM_199173	0.043	-2.12
	<i>mmp8</i> (Matrix metalloproteinase 8)	NM_002424	0.037	-2.16

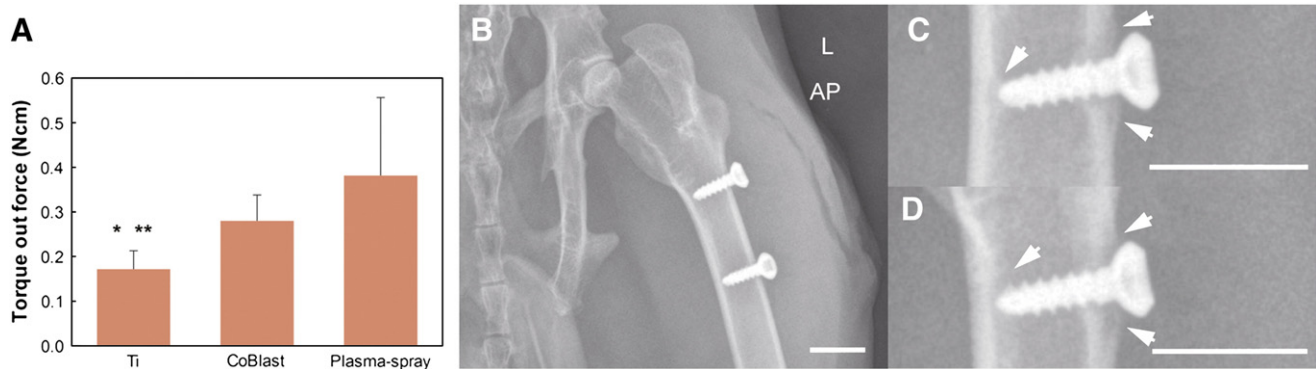


**Fig. 8.** Quantitative and qualitative analysis of *in vivo* osseointegration. **A:** Mechanical torque out force of screws removed 8 weeks after insertion (\* and \*\* indicate statistical difference when Ti vs. CoBlast and Ti vs. plasma-spray, respectively,  $P < 0.01$ ). **B:** X-ray image of the left proximal femur of an experimented New Zealand rabbit in order to demonstrate the positioning of the screws, taken immediately after insertion. **C:** X-ray image of a screw coated with CoBlast HA, 8 weeks after insertion. **D:** X-ray image of a screw coated with plasma-spray HA, 8 weeks after insertion. Scale bar = 10 mm. (L = left, AP = anteroposterior).

Osseointegration is further demonstrated by X-ray images taken 8 weeks after screw insertion. Both CoBlast HA coated (Fig. 8C) and plasma-spray HA coated screws (Fig. 8D) present with similar periosteal reaction which exhibits as thin, wavy and uniform callus formation indicated by the white arrows. In contrast to the periosteal new bone formation around the cortex which was penetrated by the screw, the bony callus over the other cortex is less prominent. The former callus should be still under remodeling at 8 weeks, and it would be expected to become thicker with time, as it is the main contributor to the torque out resistance. All in all, there is no significant visual difference between the two HA coated implants' osseointegration from X-ray images. There is no consensus regarding the effect of HA crystallinity on the cellular and tissue response. Some research propagates the argument that highly crystalline HA coating inhibits cell proliferation and osteogenic differentiation (Frayssinet et al., 1994), and low crystalline HA coating accelerates early mechanical fixation and bone ingrowth (Overgaard et al., 1999). Many others reported opposing opinions (Ball et al., 2001; Kim et al., 2005; Xue et al., 2004). The *in vitro* and *in vivo* results from our work support us to agree with the latter opinion. Nonetheless, further work needs to be done to include longer time points and also the need for a clinical trial. Since the CoBlast process offers flexible combinations of abrasive/dopant (Tan et al., 2011), what would be even more interesting is to apply various crystalline HA particles to achieve coatings covering the entire range of HA crystallinities. The results from such study are expected to be more reliable and reproducible.

### 3.6. Effects of impaction on HA *in vitro* osteoconductivity

Up to 10 impactions were applied onto the HA coatings through our simulated system, and the effect on essential material properties was first studied, then the influence on early and late cellular behavior was analyzed. After 5 and 10 impactions, CoBlast HA is still statistically less rough and more hydrophilic (Fig. 9A) than plasma-spray HA ( $P < 0.05$ ). The change of roughness by number of impactions follow a similar trend for both HA coatings: it decreases by 5 collisions ( $P < 0.05$ ), then raises dramatically ( $P < 0.001$ ) after 10 impactions, except that the initial drop in  $R_z$  for plasma-spray is much more substantial. One explanation is that 5 impactions only crush some of the peaks and thereby reduce the roughness, whereas 10 impactions might induce significant shearing effects and scrapes part of the coating off the metallic substrate. This hypothesis is consistent with the change of water contact angle with increasing number of impingements, as there is a considerable elevation of contact angle indicating a significant reduction in the coating hydrophilicity ( $P < 0.01$ ). Since unmodified Ti alloy is hydrophobic (around  $95^\circ$ ), exposure of underlying Ti after 10 impactions could render the entire

surface less hydrophilic. This is verified with EDX mapping demonstrating the coating quality change before and after 10 impactions (Fig. 9B). Both HA coatings sustained significant change afterwards with multiple noticeable friction tracks, although the damage to CoBlast is much less remarkable. Complete and partial coating detachment from basal Ti is observed on plasma-spray HA. This is in accordance with our previous *in vitro* and *in vivo* results, repeatedly substantiating the consequence of thermal degradation induced by plasma-spray process.

An overall decline in both cell attachment and mineralization for both HA coatings is noticed after 10 impactions, and this seems to be inevitable due to the coating loss (Fig. 9C). Although cell attachment on CoBlast HA is superior to that on plasma-spray HA irrespective of number of impactions, the disparity is significantly minimized after 5 impactions. Our speculation regarding an optimal roughness range could facilitate the answer here. The declined  $R_z$  could accidentally fall into its optimal range rendering it more osteoconductive for cell attachment and adhesion. Bone nodule mineralization revealed by Alizarin red staining is a strong evidence of the *in vitro* osteogenic potential of HA coatings. No statistical difference exists between CoBlast and plasma-spray either in as-received state or after 5 impactions (Fig. 5C), which is consistent with our *in vivo* osseointegration data. Interestingly, osteogenesis on CoBlast HA is significantly more pronounced compared to plasma-spray HA ( $P < 0.01$ ), which is most likely ascribed to its less impairment following impactions. The mechanism of the CoBlast HA to withstand impaction could be related to coating structure. Plasma HA is a continuous layer which can retain stress and may delaminate. However, CoBlast HA contains individual nano-crystals which are free to expand and contract thereby releasing strain and stress (O'Hare et al., 2010). It has also been suggested that substrate roughness and coating thickness may have an impact (Svehla et al., 2002). This warrants a further exploration in future work, and care also needs to be taken to preclude fractures in the metallic substrate which is thought to be the initiating factor of delamination of HA coating following stress (Lynn and DuQuesnay, 2002).

## 4. Conclusions

Hydroxyapatite has been coated onto titanium alloy implant using the novel non-thermal CoBlast process, and the resultant coating has been compared with the plasma-spray coating in terms of material property and biological response. CoBlast HA is less rough but more hydrophilic, thinner, and free of thermal effects. EDX and ICP analysis suggests that the CoBlast coating holds a higher crystallinity resulting in a slower coating dissolution in the physiological aqueous environment. *In vitro* osteoconduction and *in vivo* osseointegration analysis propose that the two HA coatings have comparable bioactivity at the cellular and

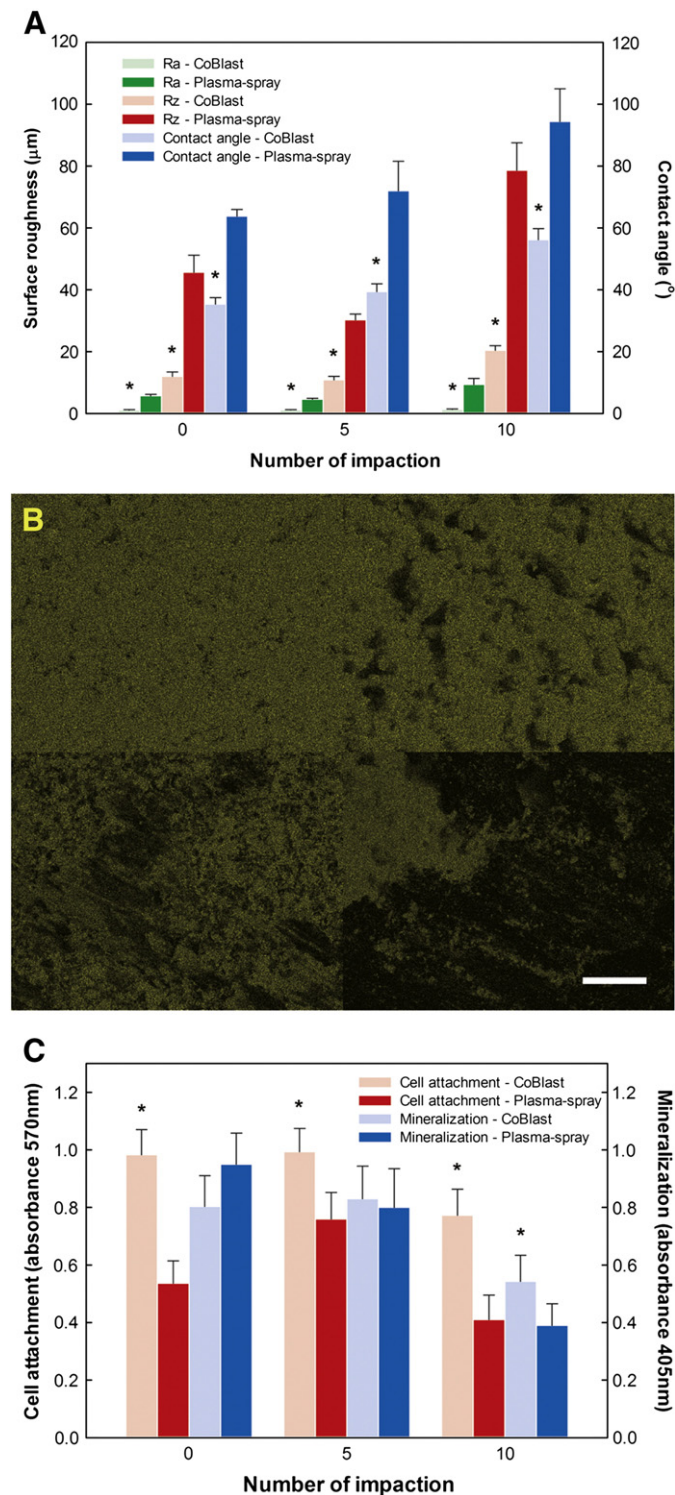


**Fig. 9.** The effect of impact on the material properties and osteoconductivity. **A:** Surface roughness and water contact angle change of the HA coatings due to impactions. **B:** EDX mapping of Ca presented in HA coatings before and after 10 impactions. Left upper = CoBlast before impaction; Right upper = plasma-spray before impaction; Left lower = CoBlast after impaction; Right lower = plasma-spray after impaction. **C:** MSCs attachment change, and *in vitro* bone mineralization change, due to impaction to the HA coatings. Scale bar = 200 µm.

tissue levels. Differentially regulated genes during osteogenesis have been identified using PCR array and validated at the protein expression level using ELISA. More importantly, CoBlast HA reserves greater tolerance to impactions allowing it to be used in more stress-prone surgical applications. Finally, the superiority of this non-thermal coating

technique makes co-deposition of growth factors or medicinal drugs achievable.

## Acknowledgements

This work was supported by Science Foundation Ireland (grant No. 08/SRC/11411). The authors would like to thank EnBIO (Cork, Ireland) for providing HA samples. We wish to thank Professor John Hunt (University of Liverpool, UK) for his generous support in initiating the *in vivo* study. Acknowledgement also goes to Dr Denis Dowling and his team (Surface Engineering Group, University College Dublin, Ireland). Finally, we would like to thank Dr Yuanqing He and his staff (Laboratory Animal Centre, Jiangsu University, China) for their help with the animal study.

## References

- Adachi N, Ochi M, Deie M, Ito Y. Transplant of mesenchymal stem cells and hydroxyapatite ceramics to treat severe osteochondral damage after septic arthritis of the knee. *J Rheumatol* 2005;32:1615–8.
- Ball MD, Downes S, Scotchford CA, Antonov EN, Bagratashvili VN, Popov VK, et al. Osteoblast growth on titanium foils coated with hydroxyapatite by pulsed laser ablation. *Biomaterials* 2001;22:337–47.
- Barry FP, Murphy JM. Mesenchymal stem cells: clinical applications and biological characterization. *Int J Biochem Cell Biol* 2004;36:568–84.
- Bilezikian J, Raisz L, Martin J. *Principles of Bone Biology*. London, UK: Academic Press; 2008.
- Canale ST, Beaty J. *Campbell's Operative Orthopaedics*. 11 ed. Missouri, USA: Mosby, Elsevier; 2007.
- Clemens JAM, Wolke JGC, Klein CPAT, de Groot K. Fatigue behavior of calcium phosphate coatings with different stability under dry and wet conditions. *J Biomed Mater Res* 1999;48:741–8.
- Compston J. Bone marrow and bone: a functional unit. *J Endocrinol* 2002;173:387–94.
- Frayssinet P, Tourenne F, Rouquet N, Conte P, Delga C, Bonel G. Comparative biological properties of HA plasma-sprayed coatings having different crystallinities. *J Mater Sci Mater Med* 1994;5:11–7.
- Gough JE, Jones JR, Hench LL. Nodule formation and mineralisation of human primary osteoblasts cultured on a porous bioactive glass scaffold. *Biomaterials* 2004;25:2039–46.
- Gregory CA, Grady Gunn W, Peister A, Prockop DJ. An Alizarin red-based assay of mineralization by adherent cells in culture: comparison with cetylpyridinium chloride extraction. *Anal Biochem* 2004;329:77–84.
- Gross KA, Berndt CC. *In vitro* testing of plasma-sprayed hydroxyapatite coatings. *J Mater Sci Mater Med* 1994;5:219–24.
- Hayashi K, Inadome T, Tsumura H, Nakashima Y, Sugioka Y. Effect of surface roughness of hydroxyapatite-coated titanium on the bone-implant interface shear strength. *Biomaterials* 1994;15:1187–91.
- Hench LL, Wilson J. *An introduction to bioceramics*. London, UK: World Scientific; 1993.
- Jaffe WL, Scott DF. *Current Concepts Review - Total Hip Arthroplasty with Hydroxyapatite-Coated Prostheses*. *J Bone Joint Surg Am* 1996;78:1918–34.
- Kazemzadeh-Narbat M, Kindrachuk J, Duan K, Jenssen H, Hancock REW, Wang R. Antimicrobial peptides on calcium phosphate-coated titanium for the prevention of implant-associated infections. *Biomaterials* 2010;31:9519–26.
- Kim H-W, Kim H-E, Salih V, Knowles JC. Sol-gel-modified titanium with hydroxyapatite thin films and effect on osteoblast-like cell responses. *J Biomed Mater Res A* 2005;74A:294–305.
- Kokubo T. *Bioceramics and Their Clinical Applications*. Abington, Cambridge, England: Woodhead Publishing Limited; 2008.
- Koshino T, Murase T, Takagi T, Saito T. New bone formation around porous hydroxyapatite wedge implanted in opening wedge high tibial osteotomy in patients with osteoarthritis. *Biomaterials* 2001;22:1579–82.
- Kweh SWK, Khor KA, Cheang P. *In vitro* investigation of plasma sprayed hydroxyapatite (HA) coatings produced with flame-spheroidized feedstock. *Biomaterials* 2002;23:775–85.
- Landor I, Vavrik P, Sosna A, Jahoda D, Hahn H, Daniel M. Hydroxyapatite porous coating and the osteointegration of the total hip replacement. *Arch Orthop Trauma Surg* 2007;127:81–9.
- Leonor IB, Alves CM, Azevedo HS, Reis RL. Effects of protein incorporation on calcium phosphate coating. *Mater Sci Eng C* 2009;29:913–8.
- Lim JY, Shaughnessy MC, Zhou Z, Noh H, Vogler EA, Donahue HJ. Surface energy effects on osteoblast spatial growth and mineralization. *Biomaterials* 2008;29:1776–84.
- Liu X, Lim JY, Donahue HJ, Dhurjati R, Mastro AM, Vogler EA. Influence of substratum surface chemistry/energy and topography on the human fetal osteoblastic cell line hFOB 1.19: Phenotypic and genotypic responses observed *in vitro*. *Biomaterials* 2007;28:4535–50.
- Livak KJ, Schmittgen TD. Analysis of Relative Gene Expression Data Using Real-Time Quantitative PCR and the 2- $[\Delta\Delta CT]$  Method. *Methods* 2001;25:402–8.
- Lynn AK, DuQuesnay DL. Hydroxyapatite-coated Ti-6Al-4V: Part 1: the effect of coating thickness on mechanical fatigue behaviour. *Biomaterials* 2002;23:1937–46.
- Moeller CW, Petruzzelli GJ, Stankiewicz JA. Hydroxyapatite-based frontal sinus obliteration. *Oper Tech Otolaryngol Head Neck Surg* 2010;21:147–9.

- Morris DC, Masuhara K, Takaoka K, Ono K, Anderson HC. Immunolocalization of alkaline phosphatase in osteoblasts and matrix vesicles of human fetal bone. *Bone Miner* 1992;19:287–98.
- Mushipe MT, Chen X, Jennings D, Li G. Cells seeded on MBG scaffold survive impaction grafting technique: Potential application of cell-seeded biomaterials for revision arthroplasty. *J Orthop Res* 2006;24:501–7.
- O'Hare P, Meenan BJ, Burke GA, Byrne G, Dowling D, Hunt JA. Biological responses to hydroxyapatite surfaces deposited via a co-incident microblasting technique. *Biomaterials* 2010;31:515–22.
- O'Neill L, O'Sullivan C, O'Hare P, Sexton L, Keady F, O'Donoghue J. Deposition of substituted apatites onto titanium surfaces using a novel blasting process. *Surf Coat Technol* 2009;204:484–8.
- Overgaard S, Bromose U, Lind M, Bunger C, Soballe K. The influence of crystallinity of the hydroxyapatite coating on the fixation of implants: mechanical and histomorphometric results. *J Bone Joint Surg Br* 1999;81-B:725–31.
- Paital SR, Dahotre NB. Calcium phosphate coatings for bio-implant applications: Materials, performance factors, and methodologies. *Mater Sci Eng R* 2009;66:1–70.
- Park J. *Bioceramics: Properties, Characterization, and Applications*. New York, USA: Springer Science+Business Media; 2008.
- Pasha R, Hill SL, Burgio DL. Evaluation of Hydroxyapatite Ossicular Chain Prostheses. *Otolaryngol Head Neck Surg* 2000;123:425–9.
- Ponsonnet L, Reybier K, Jaffrezic N, Comte V, Lagneau C, Lissac M, et al. Relationship between surface properties (roughness, wettability) of titanium and titanium alloys and cell behaviour. *Mater Sci Eng C* 2003;23:551–60.
- Quatela VC, Chow J. Synthetic Facial Implants. *Facial Plast Surg Clin North Am* 2008;16:1–10.
- Redey SA, Nardin M, Bernache-Assolant D, Rey C, Delannoy P, Sedel L, et al. Behavior of human osteoblastic cells on stoichiometric hydroxyapatite and type A carbonate apatite: Role of surface energy. *J Biomed Mater Res* 2000;50:353–64.
- Sandén B, Olerud C, Petren-Mallmin M, Larsson S. Hydroxyapatite coating improves fixation of pedicle screws: a clinical study. *J Bone Joint Surg Br* 2002;84-B:387–91.
- Setzer B, Bächle M, Metzger MC, Kohal RJ. The gene-expression and phenotypic response of hFOB 1.19 osteoblasts to surface-modified titanium and zirconia. *Biomaterials* 2009;30:979–90.
- Sun L, Berndt CC, Gross KA, Kucuk A. Material fundamentals and clinical performance of plasma-sprayed hydroxyapatite coatings: A review. *J Biomed Mater Res* 2001;58:570–92.
- Sun L, Berndt CC, Grey CP. Phase, structural and microstructural investigations of plasma sprayed hydroxyapatite coatings. *Mater Sci Eng A* 2003;360:70–84.
- Sun J-Y, Yang Y-S, Zhong J, Greenspan DC. The effect of the ionic products of Bioglass® dissolution on human osteoblasts growth cycle *in vitro*. *J Tissue Eng Regen Med* 2007;1:281–6.
- Sun J, Li J, Liu X, Wei L, Wang G, Meng F. Proliferation and gene expression of osteoblasts cultured in DMEM containing the ionic products of dicalcium silicate coating. *Biomed Pharmacother* 2009;63:650–7.
- Svehla M, Morberg P, Bruce W, Zicat B, Walsh WR. The effect of substrate roughness and hydroxyapatite coating thickness on implant shear strength. *J Arthroplasty* 2002;17:304–11.
- Tan F, Naciri M, Al-Rubeai M. Osteoconductivity and growth factor production by MG63 osteoblastic cells on bioglass-coated orthopedic implants. *Biotechnol Bioeng* 2011;108:454–64.
- Tanaka Y, Morimoto I, Nakano Y, Okada Y, Hirota S, Nomura S, et al. Osteoblasts are regulated by the cellular adhesion through ICAM-1 and VCAM-1. *J Bone Miner Res* 1995;10:1462–9.
- Tierney CM, Haugh MG, Liedl J, Mulcahy F, Hayes B, O'Brien FJ. The effects of collagen concentration and crosslink density on the biological, structural and mechanical properties of collagen-GAG scaffolds for bone tissue engineering. *J Mech Behav Biomed Mater* 2009;2:202–9.
- Tsui YC, Doyle C, Clyne TW. Plasma sprayed hydroxyapatite coatings on titanium substrates Part 2: optimisation of coating properties. *Biomaterials* 1998;19:2031–43.
- Xue W, Tao S, Liu X, Zheng X, Ding C. In vivo evaluation of plasma sprayed hydroxyapatite coatings having different crystallinity. *Biomaterials* 2004;25:415–21.
- Yuan J, Reed A, Chen F, Stewart CN. Statistical analysis of real-time PCR data. *BMC Bioinformatics* 2006;7:85.
- Zamboni G, Grano M, Greco G, Oreffo RO, Triffitt JT. Hydroxyapatite coated with insulin-like growth factor 1 (IGF1) stimulates human osteoblast activity *in vitro*. *Acta Orthop Scand* 1999;70:217–20.